Study on high voltage (5V) spinel lithium manganese oxide $LiNi_{0.5}Mn_{1.5}O_4$ by doping niobium

Wei Li[1,2,3], Xiaotao Wang[1], Dan Wu[1], Dehao Kong[1], Han Wu[1], Lai Mang[1], Bo Liao[1], O. Tegus[1,2,3], Yongjun Cao[1,2,3], Oimod Haschuluu[1,2,3]

[1]College of Physics and Electronic Information, Inner Mongolia Normal University, Hohhot 010022, Inner Mongolia, China;
[2]Inner Mongolia Key Laboratory for Physics and Chemistry of Functional Materials, Hohhot 010022, Inner Mongolia, China;
[3]Inner Mongolia Engineering Research Center for Rare Earth Functional and New Energy Storage Materials, Hohhot 010022, Inner Mongolia, China

ABSTRACT

The effect of niobium ion with high valence doping on high voltage $LiNi_{0.5}Mn_{1.5}O_4$ materials was investigated. $LiNi_{0.5}Mn_{1.5-x}Nb_xO_4$ was prepared by doping high-valent niobium ion into $LiNi_{0.5}Mn_{1.5}O_4$ material using the organic assisted combustion method. The experimental samples were characterized by scanning electron microscopy, transmission electron microscopy, X-ray diffraction, X-ray photoelectron spectroscopy and electrochemical impedance analysis. The experimental results show that the doping with high valence niobium ion change the orientation of the crystal plane growth of spinel particles, and the morphology of these particles change from the octahedral shape before doping to the spherical shape after doping. With the increase of doping amount, the crystal structure changes gradually, resulting in the $Li_{0.96}Nb_{1.01}O_3$ impurity phase. The doping of high valence niobium ion increases the content of Mn^{3+} in the material, resulting in the appearance of a 4 V discharge platform, and the formation of a 4.7 V and 4 V discharge platform. The doping of Nb can improve the cycling stability of $LiNi_{0.5}Mn_{1.5}O_4$ material, but the specific capacity of the material is reduced.

Keywords: Lithium-ion battery, High voltage spinel lithium manganate, Doping

1. INTRODUCTION

Spinel lithium manganate has the advantages of low cost and environmental protection, and can easily conduct a large current of lithium-ion, so it has a very good application prospect. Currently, a 4 V spinel lithium manganate has been commercialized in the market, but the material's low energy density has limited its large-scale development in some fields. However, 5 V high-voltage spinel $LiNi_{0.5}Mn_{1.5}O_4$ (LNMO) not only retains the advantages of $LiNi_{0.5}Mn_{1.5}O_4$, but also can improve the energy density of lithium-ion batteries with a high discharge voltage of 4.7 V, so it has become one of the most popular materials in recent years [1-4].

The cycle performance of the original material $LiNi_{0.5}Mn_{1.5}O_4$ is poor. Due to the variety of valence states of Mn ions contained in the material LNMO, especially in the

process of charging and discharging, Mn ion is easy to occur disproportionated reaction with electrolyte, which leads to deterioration of battery cycle performance. In order to further improve the cyclic stability, many researchers consider doping some other elements in the high voltage $LiNi_{0.5}Mn_{1.5}O_4$ material [5-10]. In a large number of experiments, the doped elements include Sm [11], Al [12,13], Ti [14-16], La [17], Si [18], Cr [19,20], Ga [21], etc. Among them, most of the research results show that doping can improve the cyclic stability of LNMO material. In some studies, doping also has a negative effect, the capacity of the material will decrease with the increase of doping amount.

It is found that the specific discharge capacity and cycle stability can be improved by doping 4 V spinel lithium manganate with niobium. The specific discharge capacity reaches 100 mAh g^{-1} and 80 mAh g^{-1} at 25 ℃ and 55 ℃, 2 *C* rate, respectively. It can effectively improve the cycling performance of LNMO materials [22,23]. Therefore, in this paper, niobium pentoxide was used as the doping substance to explore the influence of Nb doping on the properties of 5 V high-voltage spinel LNMO materials.

2. EXPERIMENTAL PROCESS

2.1 Preparation of LNMO and LNMO doped by Nb

The organic assisted combustion method was used to prepare the $LiNi_{0.5}Mn_{1.5-x}Nb_xO_4$ (x = 0，0.04，0.08，0.12，0.16，0.20) samples, and labeled as A-LNMO, A-LNMNO1, A-LNMNO2, A-LNMNO3, A-LNMNO4, A-LNMNO5 corresponding to different doping amounts. When synthesizing $LiNi_{0.5}Mn_{1.5-x}Nb_xO_4$, the raw materials $LiOH \cdot H_2O$, $Ni(OH)_2$, MnO_2 , and Nb_2O_5 weighed according to stoichiometric ratio are mixed with 60-90 wt.% oxalic acid at room temperature. The mixture is stirred for more than 2 hours to ensure a complete chemical reaction. The reacted slurry is then evaporated in air and further dried at 110° for more than 2 hours to obtain the precursor. Lastly, the $LiNi_{0.5}Mn_{1.5-x}Nb_xO_4$ is gained by sintering the precursor at 860 ℃ for 8 hours.

2.2 Physical property characterization method

The morphology of the sample was analyzed by JSM-5600LV scanning electron microscope. Japanese electron JEM-2100F field emitted high-resolution transmission electron microscope was used to analyze the sample surface. The accelerating voltage was 200 kV, the point resolution was 0.19 nm, and the line resolution was 0.1 nm. Differential scanning calorimeter (DSC-1150) produced by Shanghai was used to conduct differential thermal analysis of $LiNi_{0.5}Mn_{1.5}O_4$ sample precursor. EDS energy spectrum and XPS were used to analyze the element distribution and element valence state on the sample surface before and after doping.

2.3 The analysis method of electrochemical performance

The capacity and cycling performances were tested by a LAND CT-2001A multi-channel battery test system produced by Wuhanjinnuo Electronics Co., LTD. The voltage range of the test was 3.0 V~ 5.0 V, and the test current of the first charge capacity and the discharge capacity was about 0.5 *C* (1 *C*=148 mA g^{-1}). The test currently used for cyclic performance was 148 mA g^{-1}.

An electrochemical workstation (CHI660d, Shanghai Chenhua Instrument Co., LTD.) analyzes and tests AC impedance. The AC impedance test conditions were as follows: frequency scanning range of 0.01~100 kHz with an amplitude of 5 mV.

3. EXPERIMENTAL RESULTS AND DISCUSSION

3.1. Effect of Nb doping on material structure and surface morphology

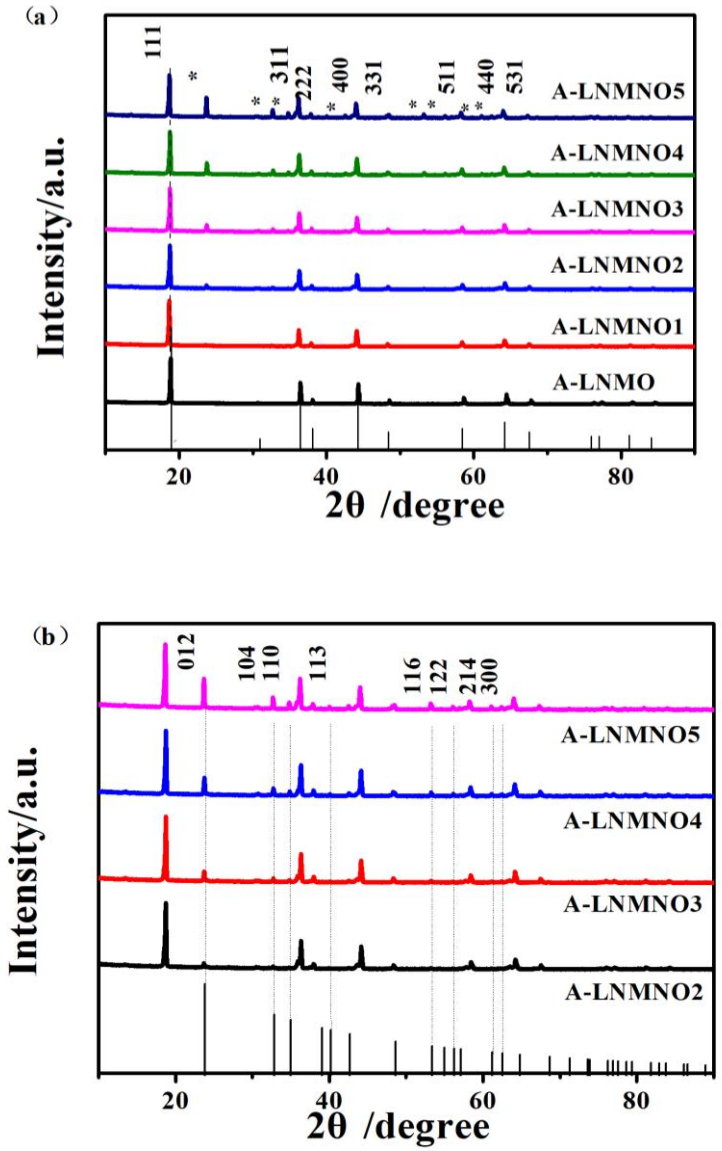

Fig. 1. X-ray diffraction patterns: (a) Identification of main phase;(b) Identification of impure phase

Table-1. The ratio of peak strength

Samples	$I_{(311)}/I_{(400)}$	$I_{(111)}/I_{(311)}$	$I_{(111)}/I_{(222)}$	$I_{(111)}/I_{(400)}$	$I_{(111)}/I_{(331)}$
A- LNMO	1.06	2.10	9.04	2.23	9.94
A-LNMNO1	1.06	2.61	9.51	2.76	11.62
A-LNMNO2	1.22	2.21	8.42	2.70	9.49
A-LNMNO3	1.26	2.19	8.03	2.75	9.52
A-LNMNO4	1.20	1.98	7.57	2.39	9.09
A-LNMNO5	1.33	1.98	7.14	2.63	9.56

Figure 1(a) shows the XRD patterns of $LiNi_{0.5}Mn_{1.5}O_4$ and $LiNi_{0.5}Mn_{1.5-x}Nb_xO_4$. By comparing the standard card, it is found that each diffraction peak position of the material A-LNMO corresponds to the crystal planes of (111) (311) (222) (400) (331) (511) (440) and (531) in the card respectively (00-035-0782). The A-LNMO sample is a typical spinel structure, and the XRD pattern is consistent with the Fd-3m space group structure[24,25]. Meanwhile, with the increase of Nb doping amount of $LiNi_{0.5}Mn_{1.5-x}Nb_xO_4$ (x=0.04 0.08 0.12 0.16 0.20), the diffraction peaks of other substances can be detected. The presence of impurity peaks indicates that the doping of Nb changes the crystal structure of $LiNi_{0.5}Mn_{1.5}O_4$. In Figure 1(b), by comparing with the card (01-083-0560), it is found that the impurity peak in the figure is $Li_{0.96}Nb_{1.01}O_3$. The appearance of the $Li_{0.96}Nb_{1.01}O_3$ peak is due to the excessive doping of niobium elements. The corresponding peak intensity ratios of crystal planes are shown in Table 1, the ratios of (311) to (400) crystal plane corresponding peak intensities of samples A-LNMO, A-LNMNO1, A-LNMNO2, A-LNMNO3, A-LNMNO4, and A-LNMNO5, $I_{(311)}/I_{(400)}$ are 1.06, 1.06, 1.22, 1.26, 1.20, and 1.33, respectively, exhibiting a gradually increasing trend. The ratios of $I_{(111)}/I_{(311)}$、$I_{(111)}/I_{(222)}$、$I_{(111)}/I_{(400)}$ and $I_{(111)}/I_{(331)}$ generally showed a downward trend, indicating that with the increase of Nb doping amount, the growth of (111) crystal plane is inhibited, and the growing trend of other crystal planes show a preferred orientation.

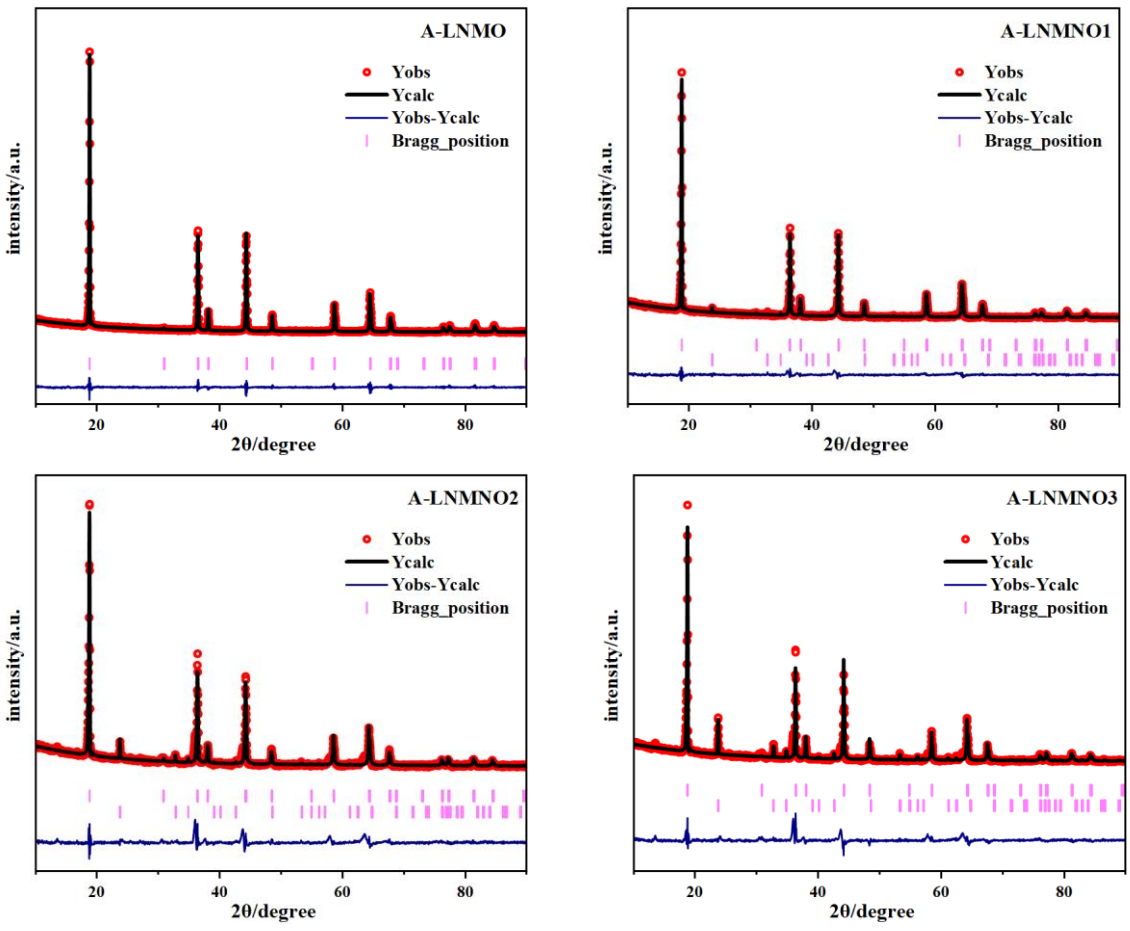

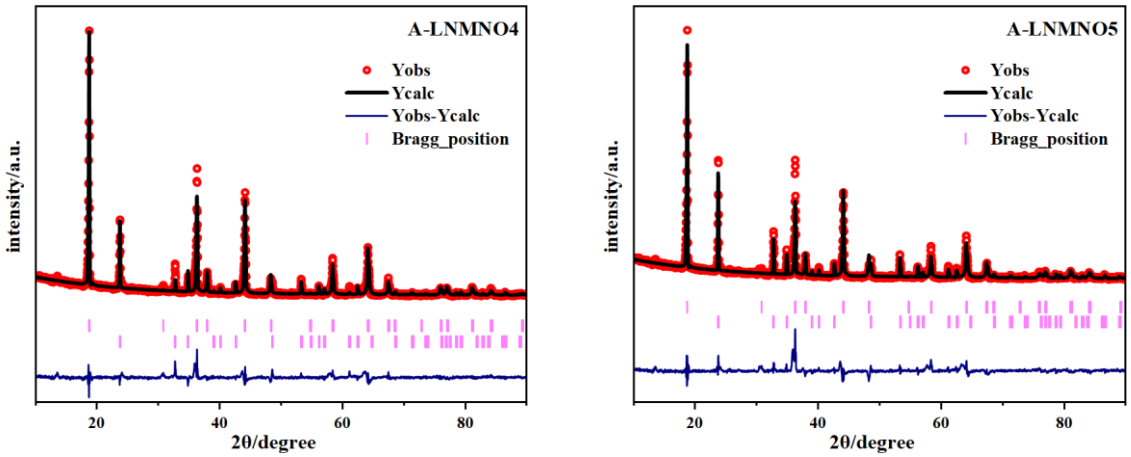

Fig.2. Full-spectrum fitting spectra of $LiNi_{0.5}Mn_{1.5-x}Nb_xO_4$

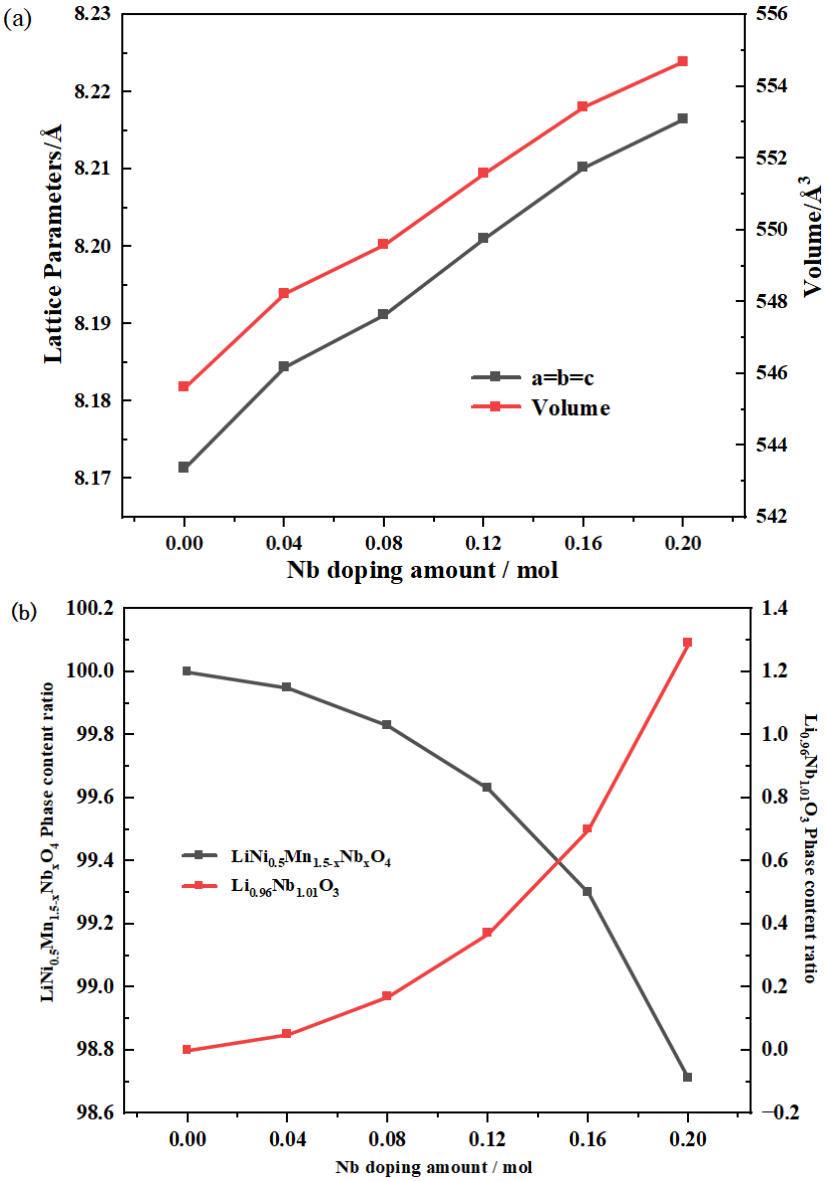

Fig.3. (a) Cell parameters and volume variation curves for different Nb doping amounts; (b) Variation curves of phase content of $LiNi_{0.5}Mn_{1.5-x}Nb_xO_4$ and $Li_{0.96}Nb_{1.01}O_3$ with different Nb doping amounts

In order to further verify the structural change of $LiNi_{0.5}Mn_{1.5}O_4$ before and after Nb doping, the Rietveld structure of $LiNi_{0.5}Mn_{1.5}O_4$ before and after Nb doping was repeatedly refined by Fullprof software. The XRD full-spectrum fitting results of samples before and after doping with different amounts of Nb are shown in Figure.2. The cell parameters, cell volume, phase content ratio and evaluation parameters of Rietveld refinement quality of $LiNi_{0.5}Mn_{1.5-x}Nb_xO_4$ (x = 0, 0.04, 0.08, 0.12, 0.16, 0.20) samples were obtained by Rietveld refinement. The values of evaluation factors R_P, R_{wp}, R_{exp}, and CHI^2 are less than 10%, indicating that the results of structural refinement are reliable [26,27,28]. Figure 3(a) shows that the cell parameters increase with the increase of Nb doping and the cell volume expands. According to the principle of electrical neutrality, it is speculated that the introduction system of Nb^{5+} promotes the change of the combined valence of Mn to maintain the charge balance, resulting in Mn^{3+}, and the ionic radius of Mn^{3+} is larger than that of Mn^{4+}. So when the amount of Nb doping in the system increases, the amount of Mn^{3+} induced will also increase, resulting in Mn^{3+} and Mn^{4+} ratio increasing, and the cell parameters and cell volume of the system will become larger [29]. Figure 3(b) illustrates that the phase content of $LiNi_{0.5}Mn_{1.5-x}Nb_xO_4$ decreases and the phase content of $Li_{0.96}Nb_{1.01}O_3$ increases with the increase of Nb doping. The decrease of $LiNi_{0.5}Mn_{1.5-x}Nb_xO_4$ phase content is considered to be the main reason for the decay of specific capacity of cathode material samples.

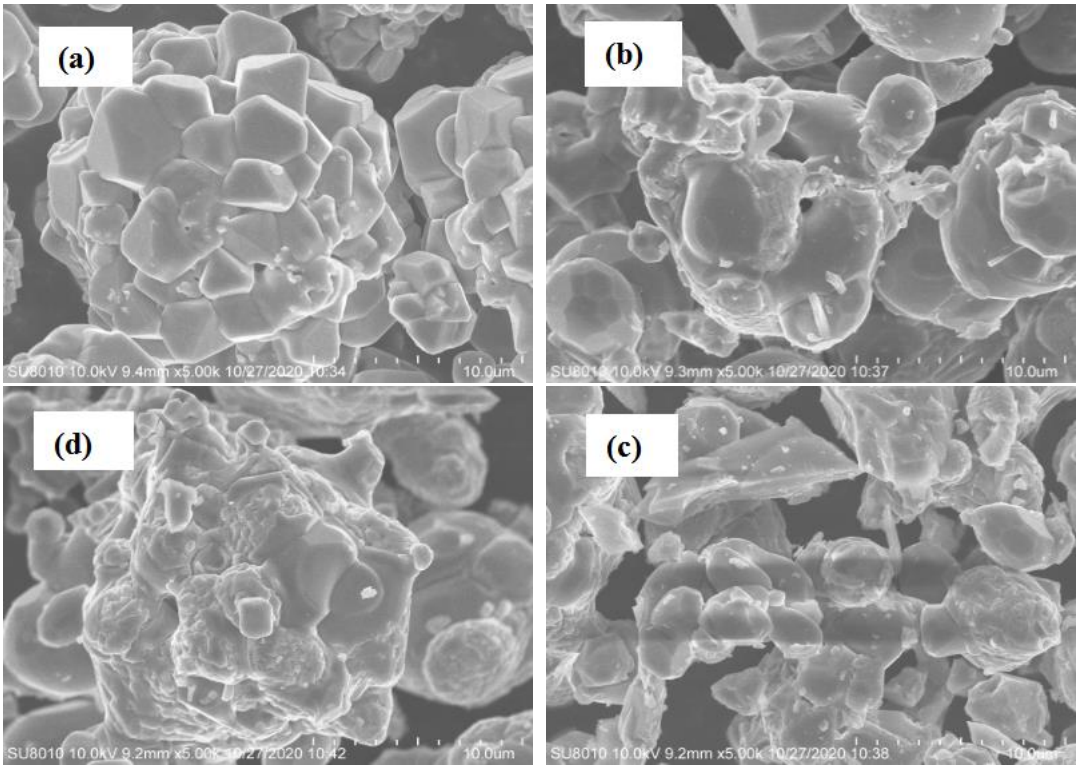

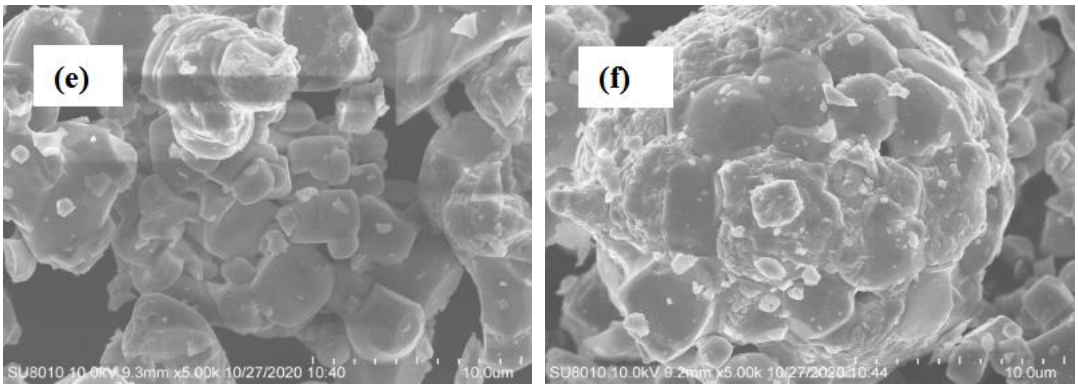

Fig. 4. SEM images of doped LNMOs; (a) A- LNMO; (b) A-LNMNO1; (c) A-LNMNO2; (d) A-LNMNO3; (e) A-LNMNO4; (f) A-LNMNO5

In order to determine the changes in the surface structure of the particles in the prepared samples, the surface morphology of $LiNi_{0.5}Mn_{1.5}O_4$ and $LiNi_{0.5}Mn_{1.5-x}Nb_xO_4$ materials before and after doping Nb was observed by scanning electron microscopy. Figure 4 shows the SEM images of the materials before and after doping. Figures (a), (b), (c), (d), (e) and (f) are the SEM images of A-LNMO、A-LNMNO1、A-LNMNO2、A-LNMNO3、A-LNMNO4、A-LNMNO5, respectively. It can be seen from the figure that the undoped sample $LiNi_{0.5}Mn_{1.5}O_4$ is an octahedral particle. The surface is flat, With the increase of doping amount, the surface structure changed obviously, and the irregular shape gradually increased. The surface of the particles are slightly uneven. The maximum size of a single particle is less than 5 μm, but an agglomeration of particles appeared, and some small particles are attached to the surface of the sample. XRD results show that with the increase of niobium doping amount, the diffraction peak intensity ratio of $I_{(311)}/I_{(400)}$, $I_{(111)}/I_{(311)}$, $I_{(111)}/I_{(222)}$, $I_{(111)}/I_{(400)}$, $I_{(111)}/I_{(331)}$ change. It is indicated that the growth of (111) crystal faces is simulated, and the growth of other crystal faces is preferentially orientated, which is the main reason for the transformation of the sample particles from octahedral shape to arc-like spherical shape.

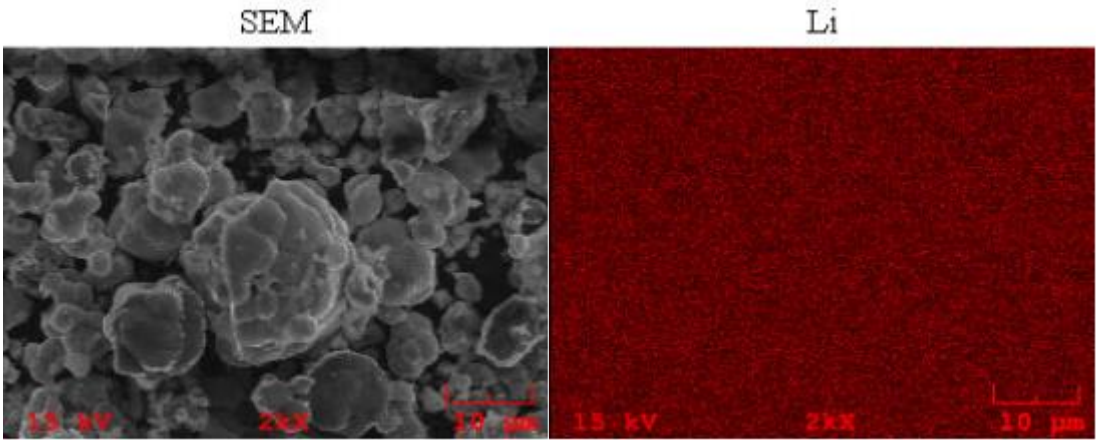

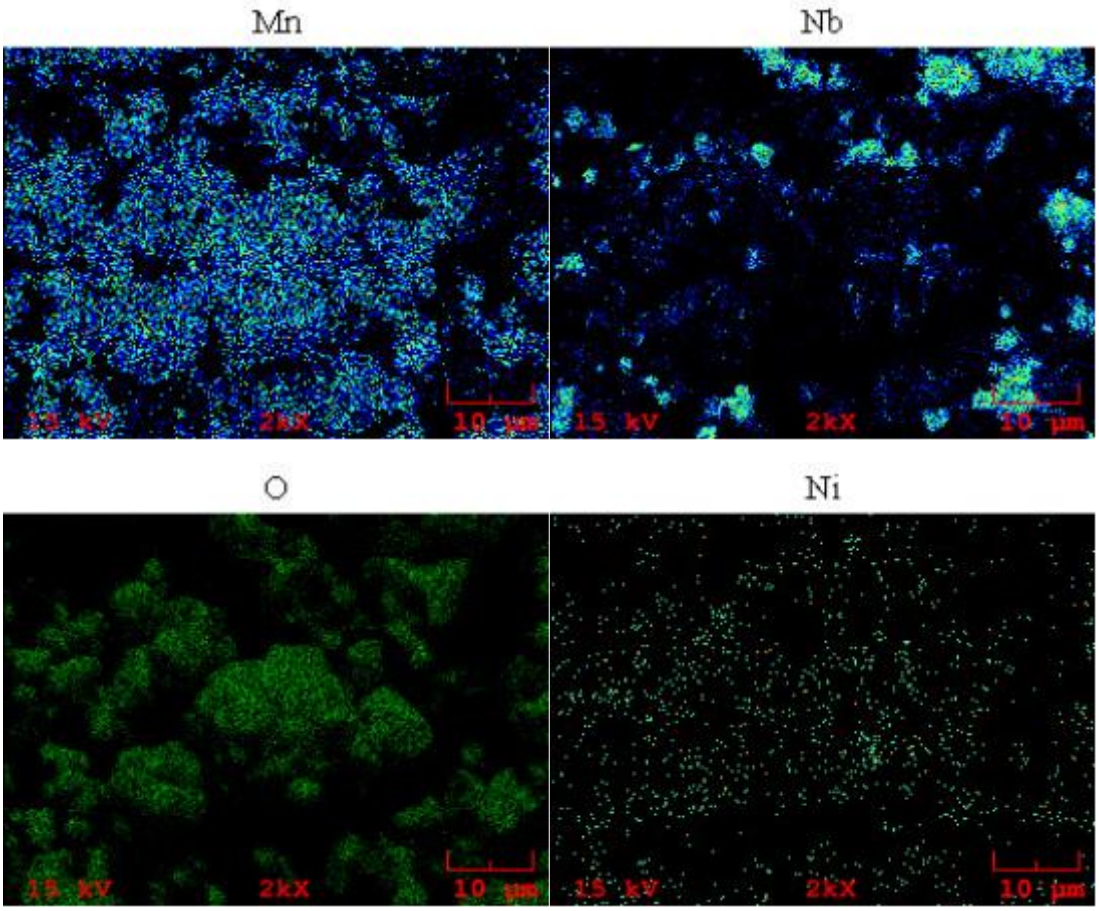

Fig. 5. EDS images of $LiNi_{0.5}Mn_{1.3}Nb_{0.2}O_4$

In order to further study whether the niobium element is uniformly doped into $LiNi_{0.5}Mn_{1.5}O_4$ material, the sample of $LiNi_{0.5}Mn_{1.3}Nb_{0.2}O_4$ was scanned. Figure 5 shows the EDS energy spectrum of $LiNi_{0.5}Mn_{1.3}Nb_{0.2}O_4$ material with the doping amount of x = 0.2. Nb element can be intuitively observed in the figure, which proves that the niobium element exists in the material powder.

Figure 5 is the EDS image of Nb-doped $LiNi_{0.5}Mn_{1.3}Nb_{0.2}O_4$ material. It can be seen from the figure that each element is distributed on the surface of particles. According to the particle distribution in the SEM figure, it can be seen that the distribution of Li element is very uniform, the distribution of Mn and Ni element is relatively uniform, the distribution of Nb element is not uniform, and there is an obvious agglomeration phenomenon, which can indicate that Nb element successfully exists in $LiNi_{0.5}Mn_{1.3}Nb_{0.2}O_4$ material, but Nb element is not uniformly mixed in $LiNi_{0.5}Mn_{1.5}O_4$. Due to the shortcomings of solid phase Nb doping, material agglomeration and bonding are easy to occur, so the internal chemical reaction is not uniform, which is also one of the problems leading to the change of the material structure.

3.2. Effect of Nb doping on elemental valence states

Figure 6 shows the XPS spectra of the materials before and after doping. Figure 6(a) shows the Ni 2p peak spectra of the materials before and after doping, Figure 6(b) shows the Mn 2p peak spectra of the materials before and after doping, and Figure 6(c) shows the Nb 3d peak spectra of the materials before and after doping. It is found that the peak spectra of Ni 2p、Mn 2p and Nb 3d are detected in the doped $LiNi_{0.5}Mn_{1.3}Nb_{0.2}O_4$ samples,

which once again proves that Nb element is doped into the high voltage $LiNi_{0.5}Mn_{1.5}O_4$ material, which is consistent with the results of EDS.

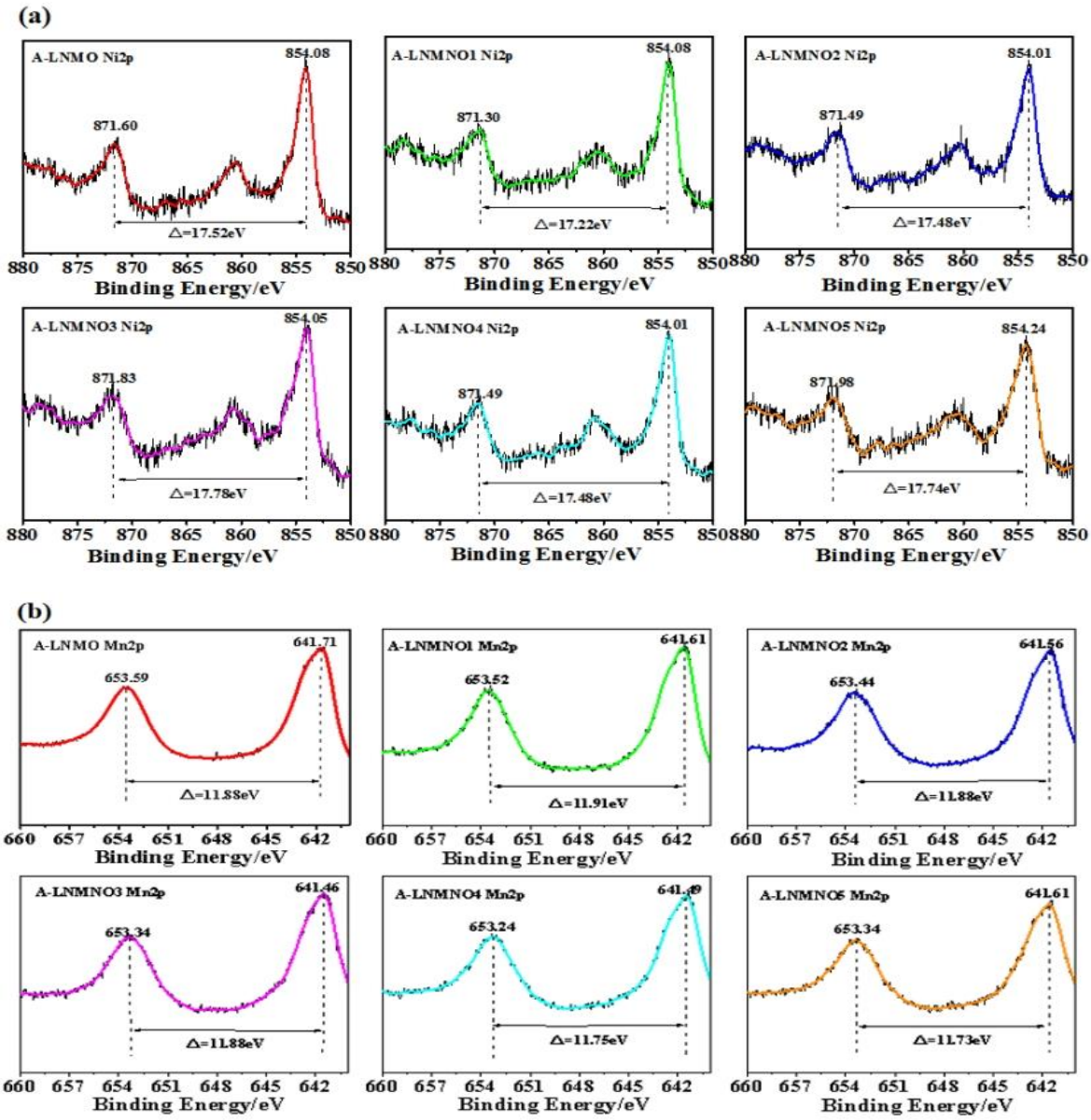

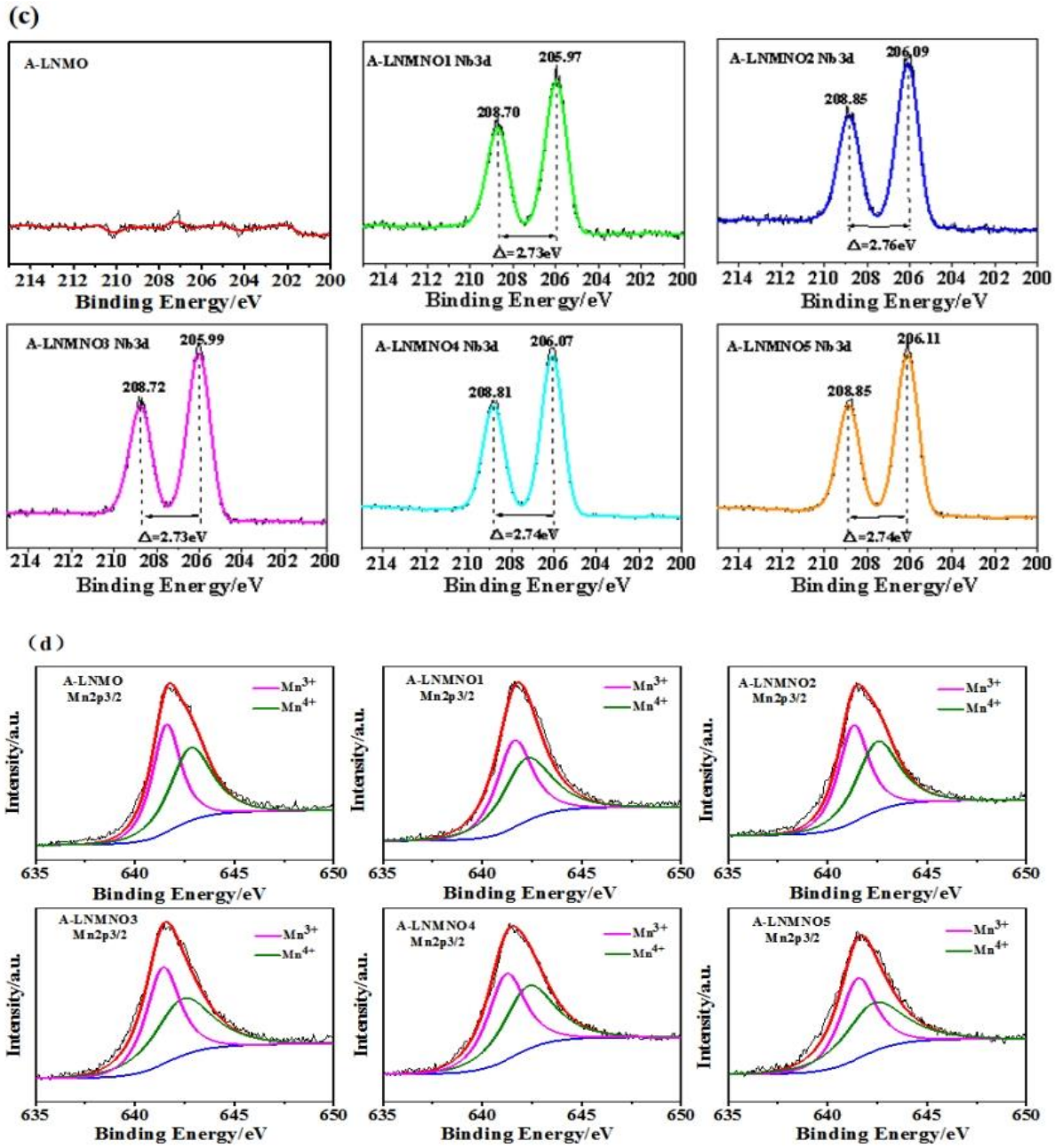

Fig. 6. XPS images of $LiNi_{0.5}Mn_{1.5}O_4$ and $LiNi_{0.5}Mn_{1.5-x}Nb_xO_4$: (a) Ni2p; (b) Mn2p; (c) Nb3d; (d) Mn2p3/2 fitting figure

As can be seen from Figure 6(a) and Figure 6(b), the binding energies of Ni 2p in $LiNi_{0.5}Mn_{1.5}O_4$ and $LiNi_{0.5}Mn_{1.3}Nb_{0.2}O_4$ are 854.08 eV、854.08 eV、854.01 eV、854.05 eV、854.01 eV、 854.24 eV, the binding energies of Mn 2p are 641.71 eV、 641.61 eV、 641.56 eV、641.46 eV、641.49 eV、641.61 eV, respectively. There are slight changes in the binding energy peak value and peak position difference value of the same element in different samples, which may be caused by the change in the valence state of the element in the Nb-doped material. Figure 6(d) shows the Mn 2p3/2 peak fitting of A-LNMO、 A-LNMNO1、A-LNMNO2、A-LNMNO3、A-LNMNO4 and A-LNMNO5 materials before and after doping. In the figure, the binding energy of each material Mn 2p3/2 is about 642 eV, and manganese ions exist in the mixed form of Mn^{3+} and Mn^{4+} [30-34]. It can be seen

from the figure that the contents of Mn^{3+} and Mn^{4+} on the surface of the sample are different before and after doping. With the increase of the niobium doping amount, the content of Mn^{3+} shows a trend of gradual increase, and part of Mn^{4+} may be converted into Mn^{3+}.

3.3. Effect of Nb doping on electrochemical performances

Figure 7 shows the first charge-discharge curves of the samples before and after doping. At room temperature, the specific discharge capacities of A-LNMO、A-LNMNO1、A-LNMNO2、A-LNMNO3、A-LNMNO4、A-LNMNO5 are 112.7 mAh g^{-1}、111.96 mAh g^{-1}、97.02 mAh g^{-1}、81.6 mAh g^{-1}、73.95 mAh g^{-1}、64.6 mAh g^{-1} respectively at 0.5*C* rate. Specific discharge capacity of Nb-doped samples decrease compared to undoped samples. With the increase of doping amount, the specific discharge capacity decreased gradually, the discharge platform of about 4 V gradually becomes wider, and the 4 V platform is generated by the redox reaction of Mn^{4+}/Mn^{3+}, indicating that with the addition of Nb element, Mn^{3+} is formed in the material, and with the increase of doping amount of Nb element, the content of Mn^{3+} increases, the proportion of 4 V platform capacity increase. This is mainly due to the presence of Nb^{5+}, which can be confirmed by the results of XPS analysis. In order to maintain valance balance in the material, part of Mn^{4+} turns into Mn^{3+}, and XRD analysis results show that Nb doping distorts the structure of spinel, and the distorted structure is not easy to conduct lithium ions. As the doping amount increases to a certain value, impure phase structure is generated in the material, so the lattice distortion and the generation of impure phase structure lead to the decrease of the specific discharge capacity of the material.

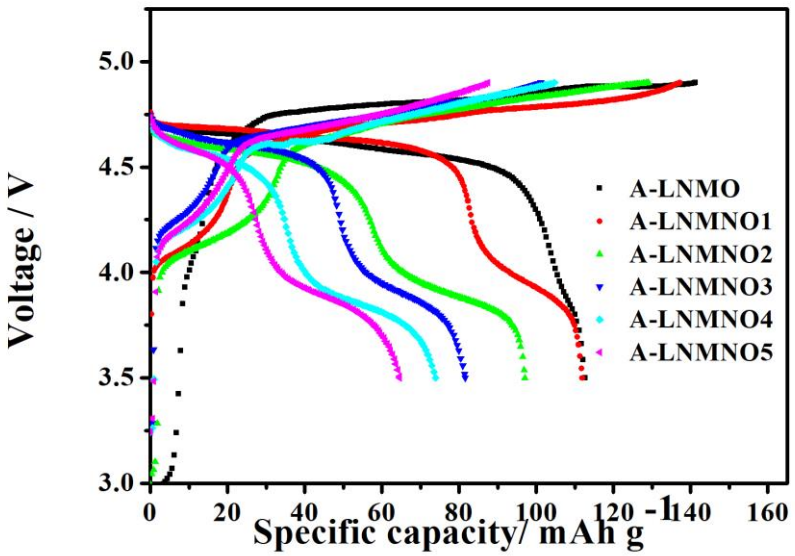

Fig. 7. Initial charge/discharge curves of LNMOs

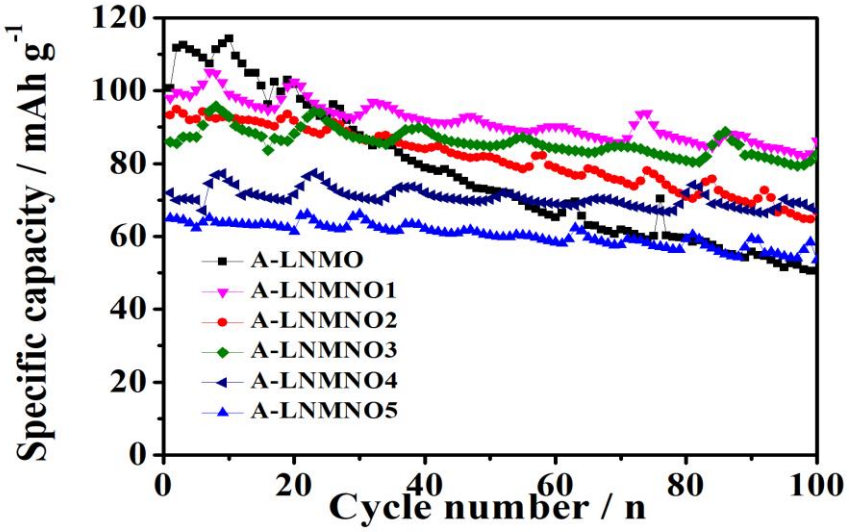

Fig. 8. Cyclic performance of LNMOs at room temperature

Figure 8 is the cycle performance curve of high voltage $LiNi_{0.5}Mn_{1.5}O_4$ material before and after doping, under the condition of constant charge and discharge current of 148 $mA.g^{-1}$ and room temperature of 25 ℃. Figure 8 shows that doping Nb improves the cyclic performance of the material at room temperature of 25 ℃. With the increase of doping amount, the retention rate of the capacity increases gradually. The specific capacity of the material gradually decreases, so it is not appropriate to increase the amount of doping substances too much, which will lead to the appearance of impurities. The change of spinel crystal structure is not conducive to the increase of capacity, but the cycling performance of the doped material is improved. Therefore, the doping of Nb shows a good capacity retention rate in this work.

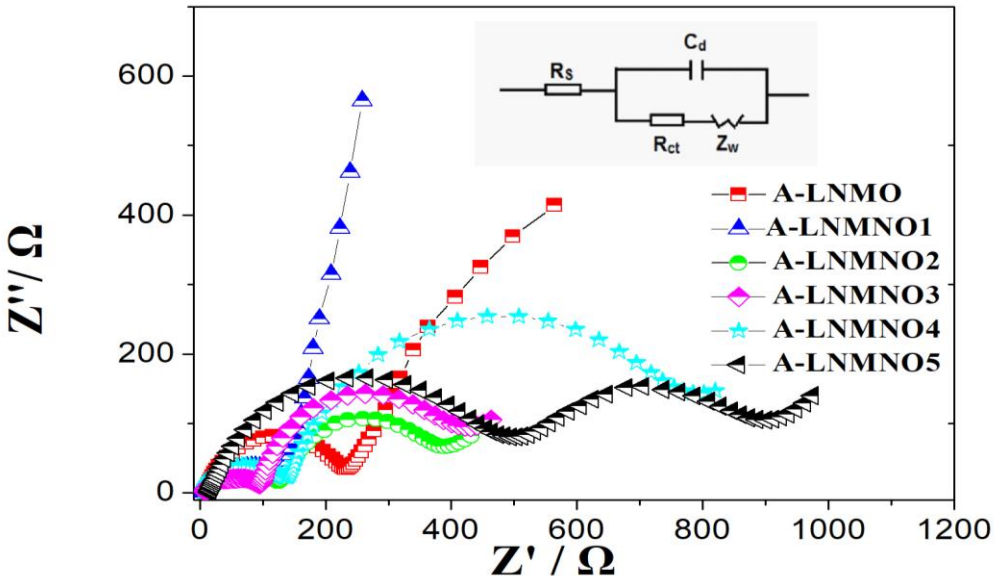

Fig. 9. EIS curve of LNMOs

Fig. 9 shows the EIS diagram of the samples at room temperature of 25 ℃. Generally, the electrochemical system of lithium ion button half battery can be represented by the equivalent circuit illustration in Figure 9, and the corresponding AC impedance spectrum is usually composed of semicircle in high frequency region and diagonal line in medium frequency region[35]. R_S represents ohmic impedance and R_{ct} represents the charge migration impedance of lithium ions at the interface of material electrochemical reaction. The intersection point of the left semicircle curve and the x-axis can be considered as R_S, and the intersection point of the right can be considered as R_{ct}[36,37].

The results in Fig. 9 show that the spectra of sample A-LNMO and sample A-LNMNO1 are composed of a semicircle and a diagonal line, which conform to the equivalent circuit model shown in Fig. 9. By comparing the spectra of sample A-LNMO and sample A-LNMNO1, it can be seen that the interface impedance between the material particle surface and the electrolyte is significantly reduced after Nb doping. With the increase of doping amount, two semicircles appear in sample A-LNMNO2, A-LNMNO3 A-LNMNO4 and A-LNMNO5 which do not conform to the analog circuit model illustrated in Fig. 9. The second semicircle in the intermediate frequency region represents the charge transfer impedance, indicating that when Nb is doped to a certain amount, the charge exchange impedance begins to appear. And with the increase of doping amount, the charge transfer impedance increases gradually. This result shows that Nb doping reduces the electrochemical reactivity of the materials. Especially when the doping amount of sample A-LNMNO5 reaches the maximum, the semicircle radius of the low frequency region increases, indicating that the interface impedance of the SEI film also increases. It can be seen from the XRD analysis results that sample A-LNMNO5 has a large amount of impurities. Because the impurities have no lithium ion deinterlacing ability, the ability of the SEI membrane at the solid-liquid interface to transport lithium ions is affected, and the interface impedance is increased.

4. CONCLUSIONS

High voltage $LiNi_{0.5}Mn_{1.5-x}Nb_xO_4$ samples doped with Nb were prepared by organic assisted combustion method. The experimental results show that Nb doping increases the crystal structure parameters of the material. The growth of (111) crystal faces is simulated, and the growth of other crystal faces is preferentially orientated after Nb doping. And Nb doping also increases the content of Mn^{3+} in the material. Nb doping reduces the specific capacity of the material, but improves the cycle performance. With the increase of doping amount, the decreasing degree of capacity also increases. The doping of high valence state Nb has a serious effect on the charging and discharging platform of the material $LiNi_{0.5}Mn_{1.5-x}Nb_xO_4$. Due to the increasing of the content of Mn^{3+}, the 4V charging and discharging platform appears, which reduces the 4.7V platform proportion of the material. An appropriate amount of Nb doping reduces the ion transfer impedance of the SEI film on the material electrode surface. With the increase of Nb doping, the charge transfer impedance will also increase.

ACKNOWLEDGMENTS

This work was financially supported by the National Natural Science Foundation of China (No. 21865021), the Inner Mongolia Key Technology Project (No. 2020GG0166), the Inner Mongolia Autonomous Region Graduate Research Innovation Project (No. S20210271Z), the Fundamental Research Funds for the Inner Mongolia Normal University (No.2022JBXC025, No.2022JBZH010, No.2022JBTD008).

REFERENCES

[1] Zhu, Z., Yan, H., Zhang, D., Li, W., Qi, L.: Preparation of 4.7V cathode material $LiNi_{0.5}Mn_{1.5}O_4$ by an oxalic acid-pretreated solid-state method for lithium-ion secondary battery. Journal of Power Sources 224(15),13-19(2013)

[2] Du, G.D., Li, NYN., Yang, J., Wang, J.L.: Fluorine-doped $LiNi_{0.5}Mn_{1.5}O_4$ for 5V cathode materials of lithium-ion battery. Materials Research Bulletin (12),3607-3613(2008)

[3] Zhong, G.B., Wang, Y.Y., Yu, Y.Q., Chen, C.H.: Electrochemical investigations of the $LiNi_{0.45}M_{0.10}Mn_{1.45}O_4$ (M= Fe, Co, Cr) 5V cathode materials for lithium-ion batteries. Journal of Power Sources 205(2012),385-393(2012)

[4] Arrebola, J.C., Caballero, A., L, Hernán., Morales, J.: Re-examining the effect of ZnO on nanosized 5V $LiNi_{0.5}Mn_{1.5}O_4$ spinel: an effective procedure for enhancing its rate capability at room and high temperatures.Journal of Power Sources 195(13),4278-4284(2010)

[5] Gao, P., Zhang, S., Ben, L.B., Zhao, W.W., Liu, Z.Z., Ribas, R., Zhu, Y.M., Huang, X.J.: Application of niobium in lithium-ion battery. Energy Storage Science and Technology 9(5), 1443-1453(2020)

[6] Fang, D.L., Li, J.C., Liu, X., Huang, P.F.: Synthesis of a Co-Ni doped $LiMn_2O_4$ spinel cathode material for high power Li-ion batteries by a solgel mediated solid state route. Journal of Alloys and Compound (640),82-89(2015)

[7] Jiang, Q.Q., Liu, D.D., Zhang, H., Wang, S.Y.: Plasma assisted sulfur doping of $LiMn_2O_4$ for high performance lithium-ion batteries. Journal of Physical Chemistry C 119(52),28776-28782(2015)

[8] Zheng, S.Q., Dou, A., Su, M.R., Liu, Y.J.: Influence of Nb Doping on Electrochemical Performance of Nanostructured Cation Disordered $Li_{1+x/100}Ni_{1/2-x/100}Ti_{1/2-x/100}Nb_{x/100}O_2$ Composites Cathode for Li-Ion Batteries. Journal of Nanoscience and Nanotechnology 20(1),452-459(2020)

[9] Li, H.L., Jian, Z.X., Yang, P.H., Li, J.J., Xing, Y.L., Zhang, S.C.: Niobium doping of $Li_{1.2}Mn_{0.54}Ni_{0.13}Co_{0.13}O_2$ cathode materials with enhanced structural stability and electrochemical performance. Ceramics International 46(15),23773-23779(2020)

[10] Wu, W., Qin, X., Guo, J.L., Wang, J.F., Yang, H.Y., Wang, L.: Influence of cerium doping on structure and electrochemical properties of $LiNi_{0.5}Mn_{1.5}O_4$ cathode materials. Journal of Rare Earths 35(09),887-895(2017)

[11] Mo, M.Y., Hui, K.S., Hong, X.T., Guo, J.S., Ye, C.C., Li, A.J., Hu, N.Q., Huang, Z.Z., Jiang, J.H., Liang, J.Z., Chen, H.Y.: Improved cycling and rate performance of Sm-doped $LiNi_{0.5}Mn_{1.5}O_4$ cathode materials for 5V lithium-ion batteries. Applied Surface Science 290(3), 412-418(2014)

[12] Luo, Y., Lu, T.L., Zhang, Y.X., Yan, L.Q., Mao, S.S., Xie, J.Y.: Surface segregated, high voltage spinel lithium-ion battery cathode material $LiNi_{0.5}Mn_{1.5}O_4$ cathodes by aluminium doping with improved high-rate cyclability. Journal of Alloys and Compounds 70, 289-297(2017)

[13] Wang, Y., Peng, Q., Yang, G., Yang, Z., Zhang, L.C., Long, H., Huang, Y.H., Lu, P.X.: High stability 5V spinel $LiNi_{0.5}Mn_{1.5}O_4$ sputtered thin film electrodes by modifying with aluminium oxide. Electrochimica Acta 136,450-456(2014)

[14] Lin, M., Wang, S.H., Gong, Z.L., Huang, X.K., Yang, Y.: A strategy to improve cyclic performance of $LiNi_{0.5}Mn_{1.5}O_4$ in a wide voltage region by Ti-doping. Journal of the Electrochemical Society 160(5), A3036-A3040(2013)

[15] Ran, Q.W., Zhao, H.Y., Hu, Y.Z., Hao, S., Liu, J.T., Li, H., Liu, X.Q.: Enhancing surface stability of $LiNi_{0.8}Co_{0.1}Mn_{0.1}O_2$ cathode with hybrid core-shell nanostructure induced by high valent titanium ions for Li-ion batteries at high cut off voltage. Journal of Alloys and Compounds 834:155099(2020)

[16] Alcantara, R., Jaraba, M., Lavela, P., Tirado, J.L.: Structural and electrochemical study of new $LiNi_{0.5}Ti_xMn_{1.5-x}O_4$ spinel oxides for 5V cathode materials. Chemistry of Materials 34(37),2376-2382(2003)

[17] Cui, X.L., Shi, X.M., Li, G.X., Li, S.Y., Xu, X.L., Li, Y.L., Mao, L.P., Ye, X.S.: Electrochemical performance of $LiNi_{0.5}Mn_{1.5}O_4$ doped with La and its compatibility with new electrolyte system. Russian Journal of Electrochemistry 50(4),363-369(2014)

[18] Keppele, M., Nageswaran, S., Kim, S.J., Srinivasan, M.: Silicon doping of high voltage spinel $LiNi_{0.5}Mn_{1.5}O_4$ towards superior electrochemical performance of lithium-ion batteries. Electrochimica Acta 213,904-910(2016)

[19] Park, S.B., Eom, W.S, Jang, H.: Electrochemical properties of $LiNi_{0.5}Mn_{1.5}O_4$ cathode after Cr doping. Journal of Power Sources 159(1),679-684(2006)

[20] Hong, K.J., Sun, Y.K.: Synthesis and electrochemical characteristics of $LiCr_xNi_{0.5-x}Mn_{1.5}O_4$ spinel as 5V cathode materials for lithium secondary batteries. Journal of Power Sources 109(2),427-430(2002)

[21] Lan, L.F., Li, S., Li, J., Lu, L., Lu, Y., Huang, S., Xu, S.J., Pan, C.Y., Zhao, F.H.: Enhancement of the electrochemical performance of the spinel structure $LiNi_{0.5-x}Ga_xMn_{1.5}O_4$ cathode material by Ga doping. Nanoscale Research Letters 13(1),251-261(2018)

[22] Pan, K.M., Hu, C., Sun, Z.Q., Xu, G.Y., Zhang, D., Yu, L.H., Wang, K.L., Jiang, K.: Structural and electrochemical characterization of $LiMn_2O_4$ and $Li_{1.05}Mn_{1.97}Nb_{0.03}O_4$ with excellent high-temperature cycling stability synthesized by a simple route. Journal of Applied Electrochemistry 50(4),451-462(2020)

[23] Xu, X.L., Deng, S.X., Wang, H., Liu, J.B., Yan, H.: Research progress in improving the cycling stability of high-voltage $LiNi_{0.5}Mn_{1.5}O_4$ cathode in lithium-ion battery. Nano-Micro Letters 9(2),1-19(2020)

[24] Kim, J.H., Myung, S.T., Yoon, C.S., Kang, S.G., Sun, Y.K.: Comparative study of $LiNi_{0.5}Mn_{1.5}O_{4-\delta}$ and $LiNi_{0.5}Mn_{1.5}O_4$ cathodes having two crystallographic structures: Fd-3m and $P4_332$. Cheminform 35(21),485-491(2004)

[25] Gao, C., Liu, H.P., Bi, S.F., Li, H.L., Ma, C.S.: Investigation the improvement of high voltage spinel $LiNi_{0.5}Mn_{1.5}O_4$ cathode material by anneal process for lithium-ion batteries. Green Energy & Environment 6(01),114-123(2021)

[26] Simoes, A.Z., Garcia, F.G., Riccardi, C.: Rietveld analysys and electrical properties of lanth anum doped $BiFeO_3$ ceramics. Materials Chemistry and Physics 116(2-3),05-309(2009)

[27] Li, H., Li, C.Q., Jiang, X.H., Wang, X., Zhi, W., Yang, Y., Lu, F.F., Yang, X.: Study on Rietveld Refinement and High-temperature Thermoelectric Properties of Dy Doped $Ca_{1-x}Dy_x$ MnO_3 (x=0,0.02,0.03,0.05,0.10) Thermoelectric Materials. Journal of Synthetic Crystals 49 (02),312-318(in Chinese)(2020)

[28] Yan, L., Qin, J.M., Liang, B.K., Gao, S.L., Wang, B., Cui, J.Y., Altan, B., Yang, Y.C.: High Pressure Rapid Synthesis of $LiCrTiO_4$ with Oxygen Vacancy for High Rate Lithium-I on Battery Anodes. Nano. micro small 2202901,1-12(2022)

[29] Flahaut, D., Mihara, T., Funahashi, R., Nabeshima, N., Lee, K., Ohta, H.: Thermoelectrical properties of a-site substituted $Ca_{1-x}Re_xMnO_3$ system. Journal of Applied Physics 100(8),23 31(2006)

[30] Yao, Y.L., Liu, H.C., Li, G.C., Peng, H.R., Chen, K.Z.: Multi-shelled porous $LiNi_{0.5}Mn_{1.5}O_4$ microspheres as a 5V cathode material for lithium-ion batteries. Materials Chemistry and Physics 143(2),867-872(2014)

[31] Quinlan, R.A., Lu, Y.C., Yang, S.H., Azzam, N., Mansour.: XPS studies of surface chemist ry changes of $LiNi_{0.5}Mn_{0.5}O_2$ electrodes during high voltage cycling. Journal of the Electroc hemical Society 160(4),A669-A677(2013)

[32] Park, J.S., Roh, K.C., Lee, J.W., Song, K., Kim, Y., Kong, Y.M.: Structurally stabilized Li $Ni_{0.5}Mn_{1.5}O_4$ with enhanced electrochemical properties through nitric acid treatment. Journal of Power Sources 230,138-142(2013)

[33] Yang, T.Y., Zhang, N.Q., Lang, Y., Sun, K.N.: Enhanced rate performance of carbon-coated $LiNi_{0.5}Mn_{1.5}O_4$ cathode material for lithium-ion batteries. Electrochimica Acta 56(11),4058-4064(2011)

[34] Yi, T.F., Hu, X.G.: Preparation and characterization of sub-micro $LiNi_{0.5-x}Mn_{1.5+x}O_4$ for 5V cathode materials synthesized by an ultrasonic-assisted co-precipitation method. Journal of P ower Sources 167(1),185-191(2007)

[35] Bredar, A. R. C., Chown, A. L., Burton, A. R., Farnum, B. H.: Electrochemical Impedance Spectroscopy of Metal Oxide Electrodes for Energy Applications. ACS Appl. Energy Mate r. 3, 66−98(2020)

[36] Lee, Y.S., Shin, W.K., Kannan, A.G., Koo, M.S., Kim, D.W.: Improvement of the cycling performance and thermal stability of lithium-ion cells by double-layer coating of cathode m aterials with Al_2O_3 nanoparticles and conductive polymer. ACS Applied Materials & Interfa ces 7(25),13944-13951(2015)

[37] Liu, T., Garsuch, A., Chesneau, F., Lucht, B.L.: Surface phenomena of high energy Li $(Ni_{1/3}Co_{1/3}Mn_{1/3})O_2$ graphite cells at high temperature and high cutoff voltages. Journal of Powe r Sources 269,920-926(2014)